

Phase separation and morphology formation in interacting ternary mixtures under evaporation – Well-posedness and numerical simulation of a non-local evolution system

Rainey Lyons^{*‡}, Emilio N. M. Cirillo[†], and Adrian Muntean[‡]

[‡]Department of Mathematics and Computer Science, Karlstad University, Sweden

[†]Department of Basic and Applied Sciences for Engineering (SBAI), Sapienza University of Rome, Italy

March 27, 2023

Abstract

We study a nonlinear coupled parabolic system with non-local drift terms modeling at the continuum level the inter-species interaction within a ternary mixture that allows the evaporation of one of the species. In the absence of evaporation, the proposed system coincides with the hydrodynamic limit of a stochastic interacting particle system of Blume–Capel–type driven by the Kawasaki dynamics. Similar governing dynamics are found in models used to study morphology formation in the design of organic solar cells, thin adhesive bands, and other applications. We investigate the well-posedness of the target system and present preliminary numerical simulations which incorporate evaporation into the model. We employ a finite volumes scheme to construct approximations of the weak solution and illustrate how the evaporation process can affect the shape and connectivity of the evolving-in-time morphologies.

Keywords: Phase separation, coupled non-local parabolic system, ternary mixture, evaporation, well-posedness, weak solutions, numerical simulation

AMS Subject classifications: 35K55, 35Q70, 65N08

1 Introduction

In this paper, we study the solvability and the numerical simulation of a nonlinear coupled parabolic system with a specific shape of the non-linear non-local drift, which is derived in [23] as hydrodynamic limit of the Blume–Capel model endowed with Kawasaki dynamics describing the interaction of ternary mixture of particles. Such mixtures typically consist of two different solutes mixed within a solvent and allow for phase separation. The situation is rather typical in modern materials science when thin films are involved; see e.g., Section 1.2 for a discussion of the application of such scenario to producing morphologies as needed for organic solar cells. In the applications discussed below, the solvent particle evaporates and plays a crucial role in the morphologies produced by the separated phases. The presence of such a non–equilibrium process makes this scenario different compared to the more classical phase separation settings arising in crystal growth, metallurgy, and so on, normally treated by Allen–Cahn–type or Cahn–Hilliard–type equations. Specifically, by controlling the evaporation mechanism a local equilibrium is frozen, i.e., one has the possibility to actively select specific morphologies as the end configuration. We refer the reader to the recent works [5, 27, 33], where this setting has been explored using Monte Carlo simulations for suitable lattice–based models. Although we are driven by these two concrete applications, our work can be seen as a continuation of the efforts started earlier by Lebowitz and Giacomin [13, 14].

*rainey.lyons@kau.se

For a good grip on the design of morphologies out of *ad hoc* polymer-polymer-solvent interactions, it is crucial to have sufficiently rich models posed at the continuum level that inherit, from the interacting particle systems, the ability to produce physically meaningful phase separation. This would set the stage for process and shape optimization operations to reach optimal macroscopic transport and reaction properties, mediated by optimal morphology shapes. However, in spite of huge efforts in the statistical mechanics and applied mathematics communities, rigorous derivations of the corresponding hydrodynamic limit equations for mixtures of interacting particle systems with evaporation are currently out of reach. The main technical difficulties in performing rigorously the hydrodynamic limit process seem to arise because of the evaporation component of the process. To allow for the evaporation of the solvent, we modify the limit system with a linear evaporation term to mimic the release of the solvent. The problem setting is relevant, with a rich phenomenology, for the presence of three coexisting phases undergoing the separation process.

1.1 Problem statement

Within this framework, the main interest is on the solvability of the following system of two coupled non-local nonlinear parabolic equations

$$\begin{cases} \partial_t m = \nabla \cdot [\nabla m - 2\beta(\phi - m^2)(\nabla J * m)] \\ \partial_t \phi = \nabla \cdot [\nabla \phi - 2\beta m(1 - \phi)(\nabla J * m)] \end{cases} \quad (t, x) \in (0, T) \times \Omega =: Q_T, \quad (1)$$

where Ω is a cube with spatially periodic boundary conditions (i.e., homeomorphic to the unit torus), T is some positive time, $\beta > 0$ is a constant representing the inverse temperature, and $J \in C_+^2(\bar{\Omega})$ is a symmetric compactly supported potential such that $\int_{\Omega} J(r) dr = 1$. For the system (1) we prescribe the initial data

$$m(t=0) = m_0 \text{ and } \phi(t=0) = \phi_0 \text{ in } \bar{\Omega}. \quad (2)$$

Additionally, we impose the following physically motivated assumption which we discuss in the next section,

$$0 \leq |m_0| \leq \phi_0 \leq 1 \text{ almost everywhere in } \bar{\Omega}. \quad (3)$$

We are particularly interested in weak solutions to the system (1).

Definition 1.1. *We say a pair $(m, \phi) \in \left(L^2(0, T; H_{\#}^1(\Omega)) \cap L^\infty(0, T; L^2(\Omega))\right)^2$ with $(\partial_t m, \partial_t \phi) \in \left(L^2(0, T; H_{\#}^{-1}(\Omega))\right)^2$ is a weak solution to (1) if $(m(t=0), \phi(t=0)) = (m_0, \phi_0)$,*

$$\int_{\Omega} \partial_t m \psi + \nabla m \cdot \nabla \psi - 2\beta(\phi - m^2)(\nabla J * m) \cdot \nabla \psi \, dx = 0,$$

and

$$\int_{\Omega} \partial_t \phi \eta + \nabla \phi \cdot \nabla \eta - 2\beta m(1 - \phi)(\nabla J * m) \cdot \nabla \eta \, dx = 0,$$

for all $(\psi, \eta) \in L^2(0, T; H_{\#}^1(\Omega)) \times L^2(0, T; H_{\#}^1(\Omega))$.

Here and throughout the paper, we use the subscript $\#$ to restrict function spaces to the subset of spatially periodic functions.

The structure of system (1) (posed for $\Omega := \mathbb{R}^d$) is derived rigorously in [23] as the hydrodynamic limit of the Kawasaki dynamics for the Blume–Capel model with range of interaction γ^{-1} , magnetic field h_1 , and chemical potential h_2 , whose Hamiltonian in a finite square $V \subset \mathbb{Z}^d$ is

$$H_\gamma(\sigma) = \frac{1}{2} \sum_{x \neq x' \in V} J_\gamma(x - x') [\sigma(x) - \sigma(x')]^2 - \sum_{x \in V} h_1 \sigma(x) - \sum_{x \in V} h_2 \sigma^2(x), \quad (4)$$

where $J_\gamma : \mathbb{R}^n \rightarrow \mathbb{R}$ is a Kac potential function, i.e.,

$$J_\gamma(r) = \gamma^d J(\gamma r) \quad (5)$$

for all $r \in \mathbb{R}^d$ and $\sigma(x) \in \{-1, 0, +1\}$ is the spin of a particle at position $x \in V$. We discuss the intuition on the discrete spin model below, but also refer the reader to the monograph [30] for more information on the context.

Our main result is the well-posedness of system (1) and the fact that the qualitative property (3) is conserved on Q_T . Particularly, we aim to prove the following theorem:

Theorem 1.1. *Let m_0, ϕ_0 be such that assumption (3) holds. Then, there exist a unique weak solution (m, ϕ) to (1) in the sense of Definition 1.1. Moreover,*

$$0 \leq |m| \leq \phi \leq 1 \text{ almost everywhere in } Q_T. \quad (6)$$

While there are many ways to prove well-posedness of system (1) using gradient flow or energy based methods (see, e.g., [12]), we aim to prove Theorem 1.1 in such a way that the addition of a ‘nice enough’ evaporation source term requires only some small adjustments. To this end, assume for a moment that solutions to (1) exist. Then the functions $w = \phi + m$ and $v = \phi - m$ would satisfy the system

$$\begin{cases} \partial_t w = \Delta w + \operatorname{div}[\beta(m-1)(\nabla J * (w-v))w] \\ \partial_t v = \Delta v + \operatorname{div}[\beta(m+1)(\nabla J * (w-v))v] \\ m = \frac{1}{2}(w-v) \end{cases}, \quad (t, x) \in Q_T. \quad (7)$$

This manipulation has revealed some hidden symmetry in our problem which turns out to be exploitable. Notice now that assumption (3) implies certain bounds on the initial data w_0, v_0 , specifically,

$$0 \leq w_0, v_0 \leq 2. \quad (8)$$

It is easy to see that existence of solutions to system (7) implies the existence of solutions to the original problem (1). Moreover, the linear nature of the transformations between the systems allow us to carry over regularity properties on (w, v) to (m, ϕ) . Also, the conservation of equation (8) for all time will imply the conservation of part of (3), namely, $0 \leq |m| \leq \phi$. This combined with an *a priori* result proven later will yield the conservation of (3) for all $t \in [0, T)$.

Equation (7) is written in a peculiar way to foreshadow our plan of attack. We aim to use a Schauder fixed-point argument to prove the existence of solutions by finding a fixed-point on the composite map

$$\mathcal{T} : \bar{m} \xrightarrow{\mathcal{T}_1} (\bar{w}, \bar{v}) \xrightarrow{\mathcal{T}_2} \frac{1}{2}(\bar{w} - \bar{v}).$$

Such arguments are common in literature, see e.g., [14] for an application to a similar equation to the first in (1) and [8] for an application to systems.

The first equation in system (1) is similar to the non-local Cahn-Hilliard equation well studied in the literature [14, 10]. In fact, it is easily seen for $\phi \equiv 1$ (i.e., a two species system), the model presented here reduces to the non-local Cahn-Hilliard equation. However, the coupling of the non-linearity to the second equation, allows for a mechanism to track the solvent ratio in the mixture. The structure of the equations in system (7) is reminiscent of equations in various applications including the McKean-Vlasov equations studied in swarms [2] and the Fokker-Planck equation studied in mean field games [20] and opinion dynamics [4, 3]. The main difference between these examples and the equations in system (7), is the non-linearity present in the drift term. While this structure is not surprising to find, as the previously mentioned McKean-Vlasov equations have been used to study interacting particle systems in different applications (e.g., [21]), this particular form of the non-linearity in the drift appears to be quite novel.

1.2 Motivating applications and microscopic interpretation

Phase separation models, such as the Cahn-Hilliard equation, have seen a wide variety of applications (see, e.g., [24]). The choice of the particular model (1) is motivated by several applications such as the formation of rubber-based zones related to the design of thin adhesive bands [6, 25]; and, the formation of morphologies in organic solar cells [18]. In both of these applications, a mixture consisting of three species of particles (two solutes and one solvent) undergoes phase separation to form the aforementioned morphologies/zones. In both applications, evaporation of the solvent plays a

key role as the ratio of solvent to the mixture has been shown to affect the resulting structure of the morphologies (see, e.g., [27] for a discrete simulation and [22] for simulations on system (1)).

Modeling the evaporation process in conjunction with phase separation is usually done at the discrete level with a Monte–Carlo simulation with the solvent particles taking some particular behavior (e.g., point–wise replacement or replacement at the boundary [5, 27, 33]). The choice of solvent behavior and spatial dimension changes the interpretation of this evaporation process. Generally for two dimensional simulations, one takes either a ‘from the top’ or a ‘from the side’ perspective. The main difficulty is finding the continuum limit of such evaporation models. Therefore, one of the goals of this manuscript is to find a way to adjust system (1), a system derived without an evaporation process, to reasonably simulate evaporation with either perspective.

Discrete lattice simulations of this behavior often assign a ‘spin’ to the particles denoted as in (4) by $\sigma(x) \in \{-1, 0, +1\}$. In this set up, the solvent particle would be assigned spin 0, while the solute particles would have spin +1 or –1. The concentration of the solution at a site x would then be represented by $|\sigma(x)|$ (traditionally in the literature as $\sigma(x)^2$). This is the measure of how much solute (independent of the spin direction) is located at a particular site.

Relating this intuition back to system (1), we let m and ϕ be continuous measures of the average spin and concentration in a given region. In the context of the discrete model, for a collection of sites $A := \{x_i\}_{i=1}^N$

$$m_A = \frac{1}{N} \sum_{i=1}^N \sigma(x_i) \text{ and } \phi_A = \frac{1}{N} \sum_{i=1}^N \sigma(x_i)^2 = \frac{1}{N} \sum_{i=1}^N |\sigma(x_i)|.$$

Therefore at this level, inequalities (3) and (6) are just applications of the triangle inequality. Since system (1) is the continuum limit of this stochastic interpretation under the Hamiltonian (4), we maintain this inequality with assumption (3).

Returning back to the continuous setting and system (1), $m : \bar{Q}_T \rightarrow \mathbb{R}$ is a function describing the net spin of particles in a given region. In other words, for a given Borel set $A \subseteq \Omega$, $\int_A m(t, x) dx$ is the net spin of particles in the set A at time t . As the spin in the Hamiltonian (4) only takes values in $\{-1, 0, +1\}$, we aim to show that $|m| \leq 1$ almost everywhere in Q_T . To capture the nuances of solvent particles, the function $\phi : \bar{Q}_T \rightarrow \mathbb{R}$ represents the concentration of solute particles, i.e., $\int_A (1 - \phi(t, x)) dx$ represents the solvent ratio in the set A at time t . Since ϕ represents the concentration, we will show that the physical inequality $0 \leq |m| \leq \phi \leq 1$ holds almost everywhere in Q_T .

1.3 Notation and organization of the paper

Positive constants whose explicit value is unimportant to the story will be denoted arbitrarily by C . If the constant depends on a particular function, f , this will be denoted by C_f . We warn that constants who share the same notation, need not share the same value.

We liberally make use of Young’s inequality for convolutions:

$$\|f * g\|_r \leq \|f\|_p \|g\|_q, \quad \text{where } \frac{1}{p} + \frac{1}{q} = 1 + \frac{1}{r}, \quad (9)$$

whenever the above norms make sense for the functions in question.

For lucidity, we use a short hand notation for spaces which appear frequently throughout the manuscript. For a given $\Omega \subset \mathbb{R}$, we define the following sets:

$$\begin{aligned} \mathcal{X} &:= L^2(0, T; H_{\sharp}^1(\Omega)) \cap L^\infty(0, T; L^2(\Omega)); \\ \mathcal{W} &:= \left\{ u \in L^2(0, T; H_{\sharp}^1(\Omega)) : \frac{d}{dt} u \in L^2(0, T; H_{\sharp}^{-1}(\Omega)) \right\}. \end{aligned}$$

The rest of paper is organized in the following way: in Section 2, we show the well–posedness of an auxiliary problem via an iteration scheme; in Section 3 we prove the existence of a fixed–point to equation (7) and complete the proof of Theorem 1.1; in Section 4 we describe a special case of how one would model the evaporation process and provide some numerical simulations. Finally, in Section 5 we conclude with some future work and some discussion on the results.

2 Analysis of auxiliary problems

Before we can show the well-posedness of system (10) (and therefore system (1)), we collect some useful auxiliary and *a priori* results. First, while *a priori* boundedness of solutions to (1) is not immediately clear, we can infer that ϕ is bounded given that m is bounded. This result will be useful to us later in showing the map $\mathcal{T} : \bar{m} \mapsto \frac{1}{2}(\bar{w} - \bar{v})$ maps bounded functions to bounded functions.

Proposition 2.1. *Let (m, ϕ) be solutions to (1) in the sense of Definition 1.1. If $|m| \leq 1$ almost everywhere in Q_T , then it also holds $\phi \leq 1$ almost everywhere in Q_T .*

Proof. Setting $\eta = [1 - \phi]^-$ the weak form of ϕ from Definition 1.1 and taking absolute values yields:

$$\frac{d}{dt} \|\eta\|_2^2 + \|\nabla \eta\|_2^2 \leq \int_{\Omega} |(2\beta m \eta \nabla J * m) \cdot \nabla \eta| dx.$$

Using Hölder and Young's inequalities, we arrive at

$$\frac{d}{dt} \|\eta\|_2^2 + \|\nabla \eta\|_2^2 \leq 2\beta^2 C_J \|\eta\|_2^2 + \frac{1}{2} \|\nabla \eta\|_2^2.$$

A standard application of the Grönwall inequality (see, e.g., [9, Chapter 7.1]) and using the fact that $\eta(t=0) \equiv 0$ implies that $\eta = [1 - \phi]^- = 0$ almost everywhere in Q_T . \square

With similar arguments and motivation, we show the following auxiliary result:

Proposition 2.2. *Assume for some $B : (0, T) \times \Omega \rightarrow \mathbb{R}$ with $\|B\|_{L^\infty(0, T; L^2(\Omega))} \leq C_B$ and $J \in C_+^2(\Omega)$, we have a weak solution $u \in L^2(0, T; H_{\sharp}^1(\Omega))$ to the equation*

$$\partial_t u = \Delta u + \operatorname{div}(B \nabla J * u), \quad (t, x) \in Q_T$$

equipped with periodic boundary conditions and where $u(t=0) = u_0$ with $|u_0| \leq C$ almost everywhere in $\bar{\Omega}$. Then, $|u| \leq C$ almost everywhere in Q_T .

Proof. From the weak form of the equation, we have for any $\eta \in L^2(0, T; H_{\sharp}^1(\Omega))$,

$$\int_{\Omega} \partial_t u \eta + \nabla u \cdot \nabla \eta + (B \nabla J * u) \cdot \nabla \eta dx = 0.$$

Letting $\eta = [u - C]^+$, we have from the above,

$$\frac{d}{dt} \|\eta\|_2^2 + \|\nabla \eta\|_2^2 = - \int_{\Omega} (B \nabla J * u) \cdot \nabla \eta dx.$$

By the assumptions on J , we have $\nabla J * C = 0$, we see that $\nabla J * u = \nabla J * (u - C)$. Therefore, using Hölder and Young's inequalities,

$$\begin{aligned} \frac{d}{dt} \|\eta\|_2^2 + \|\nabla \eta\|_2^2 &\leq \|\nabla J * \eta\|_{\infty} \|B\|_2 \|\nabla \eta\|_2 \\ &\leq \|\nabla J\|_2 \|\eta\|_2 \|B\|_2 \|\nabla \eta\|_2 \\ &\leq \frac{1}{2} C_J^2 C_B^2 \|\eta\|_2^2 + \frac{1}{2} \|\nabla \eta\|_2^2. \end{aligned}$$

A straightforward application of the Grönwall's inequality implies that $\|\eta\|_2^2 = 0$ for all $t \in (0, T)$. Repeating this argument for the test function $\psi = [u + C]^-$ implies the result. \square

2.1 Auxiliary system

In this section, we prove the following system is well-posed:

$$\begin{cases} \partial_t w = \Delta w + \operatorname{div}[B_1(\nabla J * (w - v))w] \\ \partial_t v = \Delta v + \operatorname{div}[B_2(\nabla J * (w - v))v] \end{cases}, \quad (t, x) \in Q_T, \quad (10)$$

equipped with periodic boundary conditions, where for $i = 1, 2$, $B_i : Q_T \rightarrow \mathbb{R} \in L^\infty(Q_T)$ and $w(0, x) = w_0(x)$, $v(0, x) = v_0(x)$ are bounded and nonnegative for all $x \in \bar{\Omega}$. Furthermore, we set $\int_{\Omega} w_0 dx = K_w$, $\int_{\Omega} v_0 dx = K_v$ for some $K_w, K_v \geq 0$. We understand solutions to equation (10) in the standard weak sense:

Definition 2.1. We say a pair $(w, v) \in \mathcal{X}^2$ with $(\partial_t w, \partial_t v) \in L^2(0, T; H_{\sharp}^{-1}(\Omega))^2$ is a solution to (10) if $(w(t=0), v(t=0)) = (w_0, v_0)$,

$$\int_{\Omega} \partial_t w \psi + \nabla w \cdot \nabla \psi + w B_1(\nabla J * (w - v)) \cdot \nabla \psi \, dx = 0,$$

and

$$\int_{\Omega} \partial_t v \eta + \nabla v \cdot \nabla \eta + v B_2(\nabla J * (w - v)) \cdot \nabla \eta \, dx = 0,$$

for all $(\psi, \eta) \in L^2(0, T; H_{\sharp}^1(\Omega))^2$.

Inspired by [4, 35], we use an iteration scheme method to prove the following theorem

Theorem 2.1. There exist a unique non-negative weak solution in the sense of Definition 2.1 to (10) with the following estimates

$$\|w\|_{L^\infty(0, T; L^2(\Omega))} + \|w\|_{L^2(0, T; H_{\sharp}^1(\Omega))} + \|\partial_t w\|_{L^2(0, T; H_{\sharp}^{-1}(\Omega))} \leq C_{\bar{B}, J}(\|w_0\|_2 + \|v_0\|_2),$$

and

$$\|v\|_{L^\infty(0, T; L^2(\Omega))} + \|v\|_{L^2(0, T; H_{\sharp}^1(\Omega))} + \|\partial_t v\|_{L^2(0, T; H_{\sharp}^{-1}(\Omega))} \leq C_{\bar{B}, J}(\|w_0\|_2 + \|v_0\|_2).$$

Moreover,

$$\int_{\Omega} w \, dx = K_w \text{ and } \int_{\Omega} v \, dx = K_v \text{ for all } t \in [0, T].$$

Remark. While equations in system (10) are quite similar to the equation studied by authors in [4], they fix a particular function for their convolution and do not consider additional terms in the drift. This allows them certain estimates which are not applicable in our context.

2.2 Iteration scheme

We define the iteration scheme as follows:

$$\begin{cases} \partial_t w_{n+1} = \Delta w_{n+1} + \operatorname{div}[B_1 w_{n+1} \nabla J * (w_n - v_n)] \\ \partial_t v_{n+1} = \Delta v_{n+1} + \operatorname{div}[B_2 v_{n+1} \nabla J * (w_n - v_n)] \end{cases}, \quad (t, x) \in Q_T, \quad (11)$$

where the initial conditions $w(0, x) = w_0(x)$ and $v(0, x) = v_0(x)$ are taken as the initial iteration step. We inherit all of the assumption from equation (10) and define solutions to this system in a similar manner to Definition 2.1 with the corresponding weak form:

$$\begin{cases} \int_{\Omega} \partial_t w_{n+1} \psi + \nabla w_{n+1} \cdot \nabla \psi + w_{n+1} B_1(\nabla J * (w_n - v_n)) \cdot \nabla \psi \, dx = 0 \\ \int_{\Omega} \partial_t v_{n+1} \eta + \nabla v_{n+1} \cdot \nabla \eta + v_{n+1} B_2(\nabla J * (w_n - v_n)) \cdot \nabla \eta \, dx = 0 \end{cases}. \quad (12)$$

We begin with an *a priori* result:

Lemma 2.1. Let $\{w_n\}$ and $\{v_n\}$ be sequences of solutions to (11). Then for each n ,

$$w_n, v_n \geq 0 \text{ and } \int_{\Omega} w_n \, dx = K_w, \int_{\Omega} v_n \, dx = K_v.$$

Proof. We prove this statement using mathematical induction. By the assumptions on the data w_0 and v_0 , the claim trivially holds. Now assume $w_n, v_n \geq 0$ with $\int_{\Omega} w_n \, dx = K_w, \int_{\Omega} v_n \, dx = K_v$. Testing the first equation in (12) with $\psi = [w_{n+1}]^-$, we have

$$\frac{1}{2} \frac{d}{dt} \|\psi\|_2^2 + \|\nabla \psi\|_2^2 = - \int_{\Omega} B_1 \psi \nabla J * (w_n - v_n) \cdot \nabla \psi \, dx$$

Making use of Hölder's inequality, Young's inequality, and Young's inequality for convolution we have,

$$\begin{aligned} \frac{1}{2} \frac{d}{dt} \|\psi\|_2^2 + \|\nabla\psi\|_2^2 &\leq \frac{1}{2} \|B_1 \nabla J * (w_n - v_n)\|_\infty^2 \|\psi\|_2^2 + \frac{1}{2} \|\nabla\psi\|_2^2 \\ &\leq \frac{1}{2} (C_B C_J (K_w + K_v))^2 \|\psi\|_2^2 + \frac{1}{2} \|\nabla\psi\|_2^2. \end{aligned}$$

Taking note that $\psi(0, x) \equiv 0$, the Grönwall inequality implies that $\psi \equiv 0$ in Q_T and, therefore, $w_{n+1} \geq 0$. Repeating the same calculations by testing the second equation in (12) with $\eta = [v_{n+1}]^-$ yields a similar result.

Testing equation (12) with $\psi, \eta = 1$ yields

$$\frac{d}{dt} \int_\Omega w_{n+1} dx = 0 \text{ and } \frac{d}{dt} \int_\Omega v_{n+1} dx = 0.$$

Since $w_{n+1}(0, x) = w_0(x)$ and $v_{n+1}(0, x) = v_0(x)$ we have

$$\int_\Omega w_{n+1} dx = \int_\Omega w_0 dx = K_w$$

and

$$\int_\Omega v_{n+1} dx = \int_\Omega v_0 dx = K_v$$

for all $t \in (0, T)$. □

Due to Young's convolution inequality (9), we have that the drift term in (11) is in fact uniformly bounded. Therefore, inductively applying standard Galerkin arguments found in [9, Section 7.1], we have for each n a unique solution pair $(w_{n+1}, v_{n+1}) \in \mathcal{X}^2$ in the sense of (12) and with energy estimates similar to those found in Theorem 2.1. Specifically, we have the energy estimates:

$$\|w_n\|_{L^\infty(0, T; L^2(\Omega))} + \|w_n\|_{L^2(0, T; H_\sharp^1(\Omega))} + \|\partial_t w_n\|_{L^2(0, T; H_\sharp^{-1}(\Omega))} \leq C_{\bar{B}, J} (\|w_0\|_2 + \|v_0\|_2),$$

and

$$\|v_n\|_{L^\infty(0, T; L^2(\Omega))} + \|v_n\|_{L^2(0, T; H_\sharp^1(\Omega))} + \|\partial_t v_n\|_{L^2(0, T; H_\sharp^{-1}(\Omega))} \leq C_{\bar{B}, J} (\|w_0\|_2 + \|v_0\|_2),$$

for each $n = 1, 2, \dots$

We now ensure that our scheme is convergent by proving that it builds a Cauchy sequence in a suitable space of functions.

Lemma 2.2. *There exist a $t^* > 0$ such that the sequence (w_n, v_n) is Cauchy in $L^\infty(0, t^*; L^2(\Omega))$.*

Proof. Let $\bar{w}_n := w_n - w_{n-1}$ and $\bar{v}_n := v_n - v_{n-1}$. Then from (12) we have that \bar{w}_{n+1} and \bar{v}_{n+1} satisfy the weak form:

$$\begin{cases} \int_\Omega \partial_t \bar{w}_{n+1} \psi + \nabla \bar{w}_{n+1} \cdot \nabla \psi + w_n B_1(\nabla J * (\bar{w}_n - \bar{v}_n)) \cdot \nabla \psi + \bar{w}_{n+1} B_1(\nabla J * (w_n - v_n)) \cdot \nabla \psi dx = 0 \\ \int_\Omega \partial_t \bar{v}_{n+1} \eta + \nabla \bar{v}_{n+1} \cdot \nabla \eta + v_n B_2(\nabla J * (\bar{w}_n - \bar{v}_n)) \cdot \nabla \eta + \bar{v}_{n+1} B_2(\nabla J * (w_n - v_n)) \cdot \nabla \eta dx = 0 \end{cases} \quad (13)$$

The above formulation allows us by testing with $(\psi, \eta) = (\bar{w}_{n+1}, \bar{v}_{n+1})$ to arrive at the estimates

$$\begin{cases} \frac{d}{dt} \|\bar{w}_{n+1}\|_2^2 + \|\nabla \bar{w}_{n+1}\|_2^2 = - \int_\Omega w_n B_1(\nabla J * (\bar{w}_n - \bar{v}_n)) \cdot \nabla \bar{w}_{n+1} + \bar{w}_{n+1} B_1(\nabla J * (w_n - v_n)) \cdot \nabla \bar{w}_{n+1} dx \\ \frac{d}{dt} \|\bar{v}_{n+1}\|_2^2 + \|\nabla \bar{v}_{n+1}\|_2^2 = - \int_\Omega v_n B_2(\nabla J * (\bar{w}_n - \bar{v}_n)) \cdot \nabla \bar{v}_{n+1} + \bar{v}_{n+1} B_2(\nabla J * (w_n - v_n)) \cdot \nabla \bar{v}_{n+1} dx \end{cases} \quad (14)$$

Working with the right-hand side of the first equation above we have the first integral,

$$\begin{aligned} \int_\Omega w_n B_1(\nabla J * (\bar{w}_n - \bar{v}_n)) \cdot \nabla \bar{w}_{n+1} dx &\leq \|B_1(\nabla J * (\bar{w}_n - \bar{v}_n))\|_\infty \int_\Omega |w_n \nabla \bar{w}_{n+1}| dx \\ &\leq C_{\bar{B}} C_J (\|\bar{w}_n\|_2 + \|\bar{v}_n\|_2) \|w_n\|_2 \|\nabla \bar{w}_{n+1}\|_2, \end{aligned}$$

where in the last inequality, we have used Hölder and Young's inequality for convolution. Making use of the weighted Young's inequality and the energy estimate on w_n , we can arrive at

$$\int_{\Omega} w_n B_1(\nabla J * (\bar{w}_n - \bar{v}_n)) \cdot \nabla \bar{w}_{n+1} \, dx \leq C_{\bar{B}, J, w_0, v_0} (\|\bar{w}_n\|_2^2 + \|\bar{v}_n\|_2^2) + \frac{1}{2} \|\nabla \bar{w}_{n+1}\|_2^2.$$

Looking now to the second integral, we have via Young's inequality for convolutions, Hölder's inequality, and Young's product inequality

$$\begin{aligned} \int_{\Omega} \bar{w}_{n+1} B_1(\nabla J * (w_n - v_n)) \cdot \nabla \bar{w}_{n+1} \, dx &\leq \|\nabla J * (w_n - v_n)\|_{\infty} \int_{\Omega} |\bar{w}_{n+1} \nabla \bar{w}_{n+1}| \, dx \\ &\leq C_{J, w_0, v_0} \|\bar{w}_{n+1}\|_2^2 + \frac{1}{2} \|\nabla \bar{w}_{n+1}\|_2^2. \end{aligned}$$

Repeating these calculations for \bar{v}_{n+1} , we arrive at the estimates

$$\frac{d}{dt} \|\bar{w}_{n+1}\|_2^2 + \frac{d}{dt} \|\bar{v}_{n+1}\|_2^2 \leq C_{\bar{B}, J, w_0, v_0} (\|\bar{w}_n\|_2^2 + \|\bar{v}_n\|_2^2 + \|\bar{w}_{n+1}\|_2^2 + \|\bar{v}_{n+1}\|_2^2). \quad (15)$$

Choosing t^* such that

$$\frac{C_{\bar{B}, J, w_0, v_0} t^*}{1 - C_{\bar{B}, J, w_0, v_0} t^*} < 1$$

and integrating (15) from 0 to $t < t^*$ we can arrive at the estimate

$$\|\bar{w}_{n+1}(t, \cdot)\|_2^2 + \|\bar{v}_{n+1}(t, \cdot)\|_2^2 \leq C_{\bar{B}, J, w_0, v_0, T} \left(\int_0^t \|\bar{w}_n(s, \cdot)\|_2^2 + \|\bar{v}_n(s, \cdot)\|_2^2 \, ds + \int_0^t \|\bar{w}_{n+1}(s, \cdot)\|_2^2 + \|\bar{v}_{n+1}(s, \cdot)\|_2^2 \, ds \right).$$

Taking the supremum of both sides over $[0, t^*)$, we obtain:

$$\begin{aligned} \|\bar{w}_{n+1}\|_{L^{\infty}(0, t^*; L^2(\Omega))}^2 + \|\bar{v}_{n+1}\|_{L^{\infty}(0, t^*; L^2(\Omega))}^2 &\leq C_{\bar{B}, J, w_0, v_0} \left(\|\bar{w}_n\|_{L^2(0, t^*; L^2(\Omega))}^2 + \|\bar{v}_n\|_{L^2(0, t^*; L^2(\Omega))}^2 \right. \\ &\quad \left. + \|\bar{w}_{n+1}\|_{L^2(0, t^*; L^2(\Omega))}^2 + \|\bar{v}_{n+1}\|_{L^2(0, t^*; L^2(\Omega))}^2 \right) \\ &\leq C_{\bar{B}, J, w_0, v_0} t^* \left(\|\bar{w}_n\|_{L^{\infty}(0, t^*; L^2(\Omega))}^2 + \|\bar{v}_n\|_{L^{\infty}(0, t^*; L^2(\Omega))}^2 \right. \\ &\quad \left. + \|\bar{w}_{n+1}\|_{L^{\infty}(0, t^*; L^2(\Omega))}^2 + \|\bar{v}_{n+1}\|_{L^{\infty}(0, t^*; L^2(\Omega))}^2 \right), \end{aligned}$$

where we have used the inequality

$$\|u\|_{L^2(0, t^*; L^2(\Omega))}^2 \leq t^* \|u\|_{L^{\infty}(0, t^*; L^2(\Omega))}^2. \quad (16)$$

Manipulation of the above inequality yields

$$\|\bar{w}_{n+1}\|_{L^{\infty}(0, t^*; L^2(\Omega))}^2 + \|\bar{v}_{n+1}\|_{L^{\infty}(0, t^*; L^2(\Omega))}^2 \leq \frac{C_{\bar{B}, J, w_0, v_0} t^*}{1 - C_{\bar{B}, J, w_0, v_0} t^*} \left(\|\bar{w}_n\|_{L^{\infty}(0, t^*; L^2(\Omega))}^2 + \|\bar{v}_n\|_{L^{\infty}(0, t^*; L^2(\Omega))}^2 \right), \quad (17)$$

which implies the sequence is Cauchy in $L^{\infty}(0, t^*; L^2(\Omega))$. Moreover, using inequality (16), we see this implies the sequence is also Cauchy in $L^2(0, t^*; L^2(\Omega))$. \square

Remark. The uniqueness of solutions to (10) follows from similar arguments presented in the above proof. Indeed, letting $\bar{w} = w_1 - w_2$ and $\bar{v} = v_1 - v_2$ where (w_1, v_1) and (w_2, v_2) are solutions to (10), we see that \bar{w} and \bar{v} satisfy similar equations to (13), namely

$$\begin{cases} \int_{\Omega} \partial_t \bar{w} \psi + \nabla \bar{w} \cdot \nabla \psi + w_2 B_1(\nabla J * (\bar{w} - \bar{v})) \cdot \nabla \psi + \bar{w} B_1(\nabla J * (w_1 - v_1)) \cdot \nabla \psi \, dx = 0 \\ \int_{\Omega} \partial_t \bar{v} \eta + \nabla \bar{v} \cdot \nabla \eta + v_2 B_2(\nabla J * (\bar{w} - \bar{v})) \cdot \nabla \eta + \bar{v} B_2(\nabla J * (w_1 - v_1)) \cdot \nabla \eta \, dx = 0 \end{cases}.$$

Following the calculations which lead to equation (15), we arrive at the differential inequality

$$\frac{d}{dt} \|\bar{w}\|_2^2 + \frac{d}{dt} \|\bar{v}\|_2^2 \leq C_{\bar{B}, J, w_0, v_0} (\|\bar{w}\|_2^2 + \|\bar{v}\|_2^2).$$

A standard application of Grönwall's inequality implies $\|\bar{w}\|_2^2 + \|\bar{v}\|_2^2 = 0$ for all $t \in [0, T]$.

Remark. By continuity, we can extend this argument to some maximal time T^* by first passing to the limit on the time domain $(0, t^*)$ and then reinitializing the iteration scheme with initial conditions $(w(t^*), v(t^*))$. We retroactively set $T = T^*$ throughout the paper.

Summing up, we have obtained that the constructed sequence (w_n, v_n) is fact a Cauchy sequence in $L^\infty(0, T; L^2(\Omega))^2$ (or $L^2(Q_T)^2$) and, from the energy estimates, is weakly convergent (along a subsequence) in $L^2(0, T; H_{\sharp}^1(\Omega))$ with $(\partial_t w_n, \partial_t v_n)$ weakly convergent (along a subsequence) in $L^2(0, T; H_{\sharp}^{-1}(\Omega))$. Using these results, we can pass to the limit in the weak formulation (12) (following the calculations used to derive equation (15)) as $n \rightarrow \infty$ to arrive at the weak formulation of Definition 2.1. Thus, the limit is a solution to (10).

3 The fixed-point argument

We are now ready to prove the well-posedness of equation (7) which for the reader's convenience we rewrite here:

$$\begin{cases} \partial_t w = \Delta w + \operatorname{div}[\beta(m-1)(\nabla J * (w-v))w] \\ \partial_t v = \Delta v + \operatorname{div}[\beta(m+1)(\nabla J * (w-v))v] \\ m = \frac{1}{2}(w-v) \end{cases}, \quad (t, x) \in Q_T. \quad (7)$$

Taking into account assumption (8), solutions to (7) are understood as in Definition 2.1 with $B_1 := \beta(m-1)$ and $B_2 := \beta(m+1)$. We aim to show the existence of solutions to a fixed-point to the map $\mathcal{T} : \mathcal{Z} \rightarrow \mathcal{Z}$ given by

$$\bar{m} \xrightarrow{\mathcal{T}_1} (\bar{w}, \bar{v}) \xrightarrow{\mathcal{T}_2} \frac{1}{2}(\bar{w} - \bar{v}),$$

where

$$\mathcal{Z} := \{u \in L^2(Q_T) : -1 \leq u \leq 1 \text{ almost everywhere in } Q_T\}.$$

Now, using the work done in the previous sections, we have the following lemmas:

Lemma 3.1. *The map $\mathcal{T} = \mathcal{T}_2 \circ \mathcal{T}_1$ is well-defined over the set \mathcal{Z} and $\mathcal{T} : \mathcal{Z} \rightarrow \mathcal{Z}$.*

Proof. We study separately the maps \mathcal{T}_1 and \mathcal{T}_2 .

The map \mathcal{T}_1 :

Fix $\bar{m} \in \mathcal{Z}$. By Theorem 2.1, we have the existence of a unique pair

$$(\bar{w}, \bar{v}) \in \mathcal{X}^2 \text{ with } (\partial_t \bar{w}, \partial_t \bar{v}) \in \left(L^2(0, T; H_{\sharp}^{-1}(\Omega)) \right)^2$$

such that $0 \leq \bar{w}, \bar{v}$. Thus the map \mathcal{T}_1 is well-defined.

The map \mathcal{T}_2 :

The map \mathcal{T}_2 is well-defined. What remains to be shown is that \mathcal{T}_2 maps into \mathcal{Z} . To see this, define $m := \frac{1}{2}(\bar{w} - \bar{v}) \in L^2(Q_T)$ and notice that

$$\partial_t m = \Delta m - \operatorname{div}[\beta(\bar{w} + \bar{v} - \bar{m}(\bar{w} - \bar{v}))\nabla J * m], \quad (18)$$

with $|m_0| \leq 1$. Since $\bar{m} \in L^\infty(Q_T)$, we have $\beta(\bar{w} + \bar{v} - \bar{m}(\bar{w} - \bar{v})) =: B(t, x) \in L^\infty(0, T; L^2(\Omega))$ for any $\bar{w}, \bar{v} \in L^2(0, T; H_{\sharp}^1(\Omega)) \cap L^\infty(0, T; L^2(\Omega))$. Thus, by Proposition 2.2, we have that $|m| \leq 1$. \square

Remark 3.1. *With similar arguments to those found in Proposition 2.1, it can be easily shown the function $\phi := \frac{1}{2}(\bar{w} + \bar{v})$, which satisfies the equation*

$$\partial_t \phi = \Delta \phi - \operatorname{div}[2\beta\bar{m}(1 - \phi)\nabla J * m],$$

is nonnegative and bounded by 1 (i.e., $0 \leq \phi \leq 1$) since $\bar{m}, m \in \mathcal{Z}$ and $0 \leq \bar{w}, \bar{v}$. Together, these bounds allow us to conclude $0 \leq \bar{w}, \bar{v} \leq 2$ almost everywhere in Q_T .

Lemma 3.2. *The map $\mathcal{T} = \mathcal{T}_2 \circ \mathcal{T}_1 : \mathcal{Z} \rightarrow \mathcal{Z}$ is continuous.*

Proof. Let $\bar{m}_n, \bar{m} \in \mathcal{Z}$ be such that $\bar{m}_n \rightarrow \bar{m}$ in $L^2(Q_T)$. Define also $(\bar{w}_n, \bar{v}_n) := \mathcal{T}_1(m_n)$ and $(\bar{w}, \bar{v}) := \mathcal{T}_1(m)$. We want to show $(\bar{w}_n, \bar{v}_n) \rightarrow (\bar{w}, \bar{v})$ in $L^2(Q_T)$. To this end, let $m := \bar{m}_n - \bar{m}$, $w := \bar{w}_n - \bar{w}$, and $v := \bar{v}_n - \bar{v}$ for fixed n . Following similar manipulations which gave rise to equation (13), we have that w and v satisfy

$$\left\{ \begin{array}{l} \int_{\Omega} \partial_t w \psi + \nabla w \cdot \nabla \psi \, dx = - \int_{\Omega} \beta \bar{w}_n (\bar{m}_n - 1) (\nabla J * (w - v)) \cdot \nabla \psi + w (\bar{m}_n - 1) (\nabla J * (\bar{w} - \bar{v})) \cdot \nabla \psi \, dx \\ \quad - \int_{\Omega} \bar{w} m (\nabla J * (\bar{w} - \bar{v})) \cdot \nabla \psi \, dx \\ \int_{\Omega} \partial_t v \eta + \nabla v \cdot \nabla \eta \, dx = - \int_{\Omega} \beta \bar{v}_n (\bar{m}_n + 1) (\nabla J * (w - v)) \cdot \nabla \eta + v (\bar{m}_n + 1) (\nabla J * (\bar{w} - \bar{v})) \cdot \nabla \eta \, dx \\ \quad - \int_{\Omega} \bar{v} m (\nabla J * (\bar{w} - \bar{v})) \cdot \nabla \eta \, dx \end{array} \right. \quad (19)$$

Testing with $(\psi, \eta) = (w, v)$ we have the following equations:

$$\left\{ \begin{array}{l} \frac{d}{dt} \|w\|_2^2 + \|\nabla w\|_2^2 = - \int_{\Omega} \beta \bar{w}_n (\bar{m}_n - 1) (\nabla J * (w - v)) \cdot \nabla w + w (\bar{m}_n - 1) (\nabla J * (\bar{w} - \bar{v})) \cdot \nabla w \, dx \\ \quad - \int_{\Omega} \bar{w} m (\nabla J * (\bar{w} - \bar{v})) \cdot \nabla w \, dx \\ \frac{d}{dt} \|v\|_2^2 + \|\nabla v\|_2^2 = - \int_{\Omega} \beta \bar{v}_n (\bar{m}_n + 1) (\nabla J * (w - v)) \cdot \nabla v + v (\bar{m}_n + 1) (\nabla J * (\bar{w} - \bar{v})) \cdot \nabla v \, dx \\ \quad - \int_{\Omega} \bar{v} m (\nabla J * (\bar{w} - \bar{v})) \cdot \nabla v \, dx \end{array} \right. \quad (20)$$

Making use of Remark 3.1, the first two terms on the right-hand side of both equations can be handled as in the proof of Lemma 2.2 to arrive at the bounds:

$$\left\{ \begin{array}{l} \left| \int_{\Omega} \beta [\bar{w}_n (\bar{m}_n - 1) (\nabla J * (w - v)) + w (\bar{m}_n - 1) (\nabla J * (\bar{w} - \bar{v}))] \cdot \nabla w \, dx \right| \leq C_J (\|w\|_2^2 + \|v\|_2^2) + \frac{1}{3} \|\nabla w\|_2^2 \\ \left| \int_{\Omega} \beta [\bar{v}_n (\bar{m}_n + 1) (\nabla J * (w - v)) + v (\bar{m}_n + 1) (\nabla J * (\bar{w} - \bar{v}))] \cdot \nabla v \, dx \right| \leq C_J (\|w\|_2^2 + \|v\|_2^2) + \frac{1}{3} \|\nabla v\|_2^2 \end{array} \right. \quad (21)$$

Meanwhile, the new third term yields the bound

$$\left\{ \begin{array}{l} \left| \int_{\Omega} \bar{w} m (\nabla J * (\bar{w} - \bar{v})) \cdot \nabla w \, dx \right| \leq C_J \|m\|_2^2 + \frac{1}{3} \|\nabla w\|_2^2 \\ \left| \int_{\Omega} \beta \bar{v} m (\nabla J * (\bar{w} - \bar{v})) \cdot \nabla v \, dx \right| \leq C_J \|m\|_2^2 + \frac{1}{3} \|\nabla v\|_2^2 \end{array} \right. \quad (22)$$

Summing up the two inequalities and maximizing constants leaves us with

$$\frac{d}{dt} \|w\|_2^2 + \frac{d}{dt} \|v\|_2^2 \leq C_J (\|m\|_2^2 + \|w\|_2^2 + \|v\|_2^2). \quad (23)$$

Integrating the above equation from 0 to t gives us the integral inequality

$$\|w\|_2^2 + \|v\|_2^2 \leq C_J \|m\|_{L^2((0,t) \times \Omega)}^2 + C_J \int_0^t (\|w\|_2^2 + \|v\|_2^2) \, ds. \quad (24)$$

Grönwall's inequality and integration provides us with the estimate:

$$\|w\|_{L^2(Q_T)}^2 + \|v\|_{L^2(Q_T)}^2 \leq C_J T \|m\|_{L^2(Q_T)}^2 \exp(C_J T). \quad (25)$$

Continuity follows of \mathcal{T}_1 and therefore \mathcal{T} follows. \square

Theorem 3.1. *The map $\mathcal{T} := \mathcal{T}_2 \circ \mathcal{T}_1$ has at least one fixed-point $m^* \in \mathcal{W} \cap \mathcal{Z}$.*

Proof. Summing up the results from before, we have the set \mathcal{Z} is a non-empty, closed, and convex subset of $L^2(Q_T)$, the map $\mathcal{T} : \mathcal{Z} \rightarrow \mathcal{Z}$ is well-defined and continuous (Lemmas 3.1 and 3.2), and $\mathcal{T}(\mathcal{Z}) \subseteq \mathcal{W}$ which is compactly embedded in $L^2(Q_T)$ via Lions-Aubin’s Lemma. Therefore, we can employ Schauder’s Fixed-Point Theorem to conclude there exists a fixed-point in $\mathcal{W} \cap \mathcal{Z}$. \square

Summing up, we have shown the existence of bounded solutions (w, v) to problem (7). By manipulation, we can see that the functions $m = \frac{1}{2}(w - v)$ and $\phi = \frac{1}{2}(w + v)$ are solutions to equation (1). Moreover, we have shown that $0 \leq w, v \leq 2$ which implies that

$$|m| \leq \phi.$$

Since in the fixed-point argument we show that $m \in \mathcal{Z}$, we can conclude via Proposition 2.1 that $\phi \leq 1$. Thus we have shown the existence of bounded solutions to equation (1) in the sense of Definition 1.1. A proof of the uniqueness of bounded solutions can be found in [23]. This proves Theorem 1.1.

4 Including evaporation: A simple example

Looking at a thin film, modeling the evaporation of the solvent phase from a mixture of multiple phases interacting among themselves as well as with the solvent, is, in general, quite complicated. Consequently, accurate quantitative predictions are usually out of reach. However, in an experimentally controlled setup with not too many interacting phases and where the effect of temperature gradients can be neglected, valuable qualitative insights can be reached. For instance, in the context of applications to organic solar cells, the solvent evaporates into vapor and moves up and leaves the film. This process leaves us with two perspectives on the actual geometry of the thin film: from ‘the side’ and from ‘the top’. For continuum models, the side perspective of the evaporation process can be modeled as a moving interface separating the solvent vapor and liquid phases as done, for instance, in [7]. This process tends to result in the formation of solvent ‘lanes’ and can be observed both in continuum [7] models as well as in discrete lattice models [33]. On the other hand, an observer of the top view of the film would see a bulk evaporation which is usually modeled as right-hand side source term of a balance law for solvent posed in two dimensions and not as a moving-boundary condition imposed on a moving surface within the thin film. Such situation is conceptually simpler and is easier to handle from modeling, mathematical analysis, and simulation points of view.

In this section, we tackle the ‘from the top’ perspective and leave both ‘the side’ perspective and the combination of the two in three dimensions as future work. To this end, we limit our spatial dimension to 2 and simulate a perspective of evaporation of the solvent component ‘from the top’ with a source term on the right-hand side of the ϕ equation namely

$$\begin{cases} \partial_t m = \nabla \cdot [\nabla m - 2\beta(\phi - m^2)(\nabla J * m)] & (t, x) \in (0, T) \times \Omega =: Q_T \\ \partial_t \phi = \nabla \cdot [\nabla \phi - 2\beta m(1 - \phi)(\nabla J * m)] + F(\phi) \end{cases} \quad (26)$$

with all assumptions on data still in place (cf. section 2). For the function F to make sense as an evaporation term for solvent, we assume that $F : \mathbb{R} \rightarrow \mathbb{R}$ is a bounded non-increasing function with $F(1) = 0$. In other words, the rate of solvent evaporation is expected to be decreasing with respect to the concentration and there should be no evaporation in areas where no solvent is present. Obviously with such a source term, the conservation of mass properties enjoyed in sections 2 and 3 will be replaced by an inequality.

The arguments employed in section 2 and section 3 can be reused to show well-posedness of (26) endowed with periodic boundary conditions under some additional mild restrictions on F . For example, a sufficient property of F is the estimate

$$\left| \int_{\Omega} F\left(\frac{1}{2}(w + v)\right)(w + v) \, dx \right| \leq C_F(1 + \|w\|_2^2 + \|v\|_2^2).$$

4.1 Simulation results

To fix ideas, we take into account a linear evaporation model, i.e., $F : \mathbb{R} \rightarrow \mathbb{R}$ defined by $F(r) = \alpha(1 - r)$ for all $r \in \mathbb{R}$ with given $\alpha > 0$. We refer the reader to section 2.4.3.3 in [26] for a motivation of this particular structure that describes in a very simplified way the liquid-gas transition. More information

on how to include the evaporation mechanism in models capturing phase separation in thin films can be found e.g. in [32].

We use a finite volume scheme similar to that presented in [22] with slight modifications to include the production term by evaporation. Namely, for fixed mesh sizes $\Delta t, \Delta x, \Delta y > 0$ we discretize the initial pair (m_0, ϕ_0) with the approximations

$$m_{i,j}^0 := \frac{1}{|\Lambda_{i,j}|} \int_{\Lambda_{i,j}} m_0(x, y) dx dy \quad \text{and} \quad \phi_{i,j}^0 := \frac{1}{|\Lambda_{i,j}|} \int_{\Lambda_{i,j}} \phi_0(x, y) dx dy$$

and define the fully explicit scheme:

$$\left\{ \begin{array}{l} \frac{m_{i,j}^{k+1} - m_{i,j}^k}{\Delta t} = \frac{1}{\Delta x^2} D_i^2[m_{i,j}^k] + \frac{1}{\Delta y^2} D_j^2[m_{i,j}^k] \\ \quad - \frac{\beta}{\Delta x} D_i^1[(\phi_{i,j}^k - (m_{i,j}^k)^2) \tilde{J}_{x,i,j}^k] - \frac{\beta}{\Delta y} D_j^1[(\phi_{i,j}^k - (m_{i,j}^k)^2) \tilde{J}_{y,i,j}^k] \\ \frac{\phi_{i,j}^{k+1} - \phi_{i,j}^k}{\Delta t} = \frac{1}{\Delta x^2} D_i^2[\phi_{i,j}^k] + \frac{1}{\Delta y^2} D_j^2[\phi_{i,j}^k] \\ \quad - \frac{\beta}{\Delta x} D_i^1[m_{i,j}^k(1 - \phi_{i,j}^k) \tilde{J}_{x,i,j}^k] - \frac{\beta}{\Delta y} D_j^1[m_{i,j}^k(1 - \phi_{i,j}^k) \tilde{J}_{y,i,j}^k] + F(\phi_{i,j}^k) \end{array} \right. ,$$

where

$$D_l^2[f_l] := f_{l+1} - 2f_l + f_{l-1}, \quad D_l^1[f_l] := f_{l+1} - f_{l-1},$$

and $\tilde{J}_{x,i,j}^k$ (respectively, $\tilde{J}_{y,i,j}^k$) denotes the approximation of $\partial_x J * m^k(x_i, y_j)$ (respectively, $\partial_y J * m^k(x_i, y_j)$) using a fast Fourier transform method similar to [34]. We remark that similar estimates to those found in Section 2 can be repurposed to discuss convergence of the finite volume scheme.

As in [22], we observe morphology formation during the simulation. However, whereas in the previous results the shape-type (e.g., ‘ball-like’ or ‘bi-continuous’) of morphologies stays consistent throughout the simulation, we observe a change in shape-type while there is an evaporation component. This phenomenon is demonstrated in Figure 1 where ‘ball-like’ structures can be seen at early times ($t = 1$) and they slowly grow as solvent evaporates in to long continuous structures at later times. A similar situation pointing out a competition between phase separation and evaporation is reported in [31]. Here the shapes of the morphologies formed in a partially miscible mixture change during the evaporation process, while one notes that the spinodal instability occurs when the evaporation is fast.

In Figure 2, we present multiple measurements of the simulation. First, we present the ratio of solvent during the simulation over time given by $\|1 - \phi\|_1$. As expected, we observe a decrease in solvent ratio over time. Next, we plot the $\|\cdot\|_1$ norms of both m and ϕ (scaled by the norm of the initial condition) over time. The observed behavior is an increase in total volume of the solute. This is reminiscent of the Monte-Carlo simulation of somewhat related microscopic models (see [27, 5]), where the evaporating solvent was replaced by solute particles. We note that the sudden drop in the L^1 norm of m is due to the initial mixing of the solution (ternary mixture). In other words, this drop happens during the time period where morphologies are not yet well formed. In the aforementioned cited papers, the evaporating solvent was replaced by solute in such a way that the ratio of +1 and -1 particles was kept constant. We measure this effect in the third plot of Figure 2 where we plot the evolution of the ratio of $\|m^+\|_1$ and $\|m^-\|_1$. Here, we observe an approximate 4% variance of this ratio due to the numerical scheme. However, it appears to self correct over time.

5 Discussion and outlook

Summarizing our work here, we have shown the existence of a unique bounded solution to system (1) with standard parabolic regularity for some finite time. Moreover, the solutions to this system conserve the physical inequality (6). We have included an example of how to adjust system (1) to include a ‘from the top’ evaporation process and included simulations of a simple example of this process. While the particular example of evaporation is simple, clear transitions between the patterns studied in [22] can be observed in Figure 1.

The study of such type of phase separation models is rich with questions and it remains to be seen how the analysis of similar models such as the Cahn–Hilliard and Allen–Cahn equations compare to

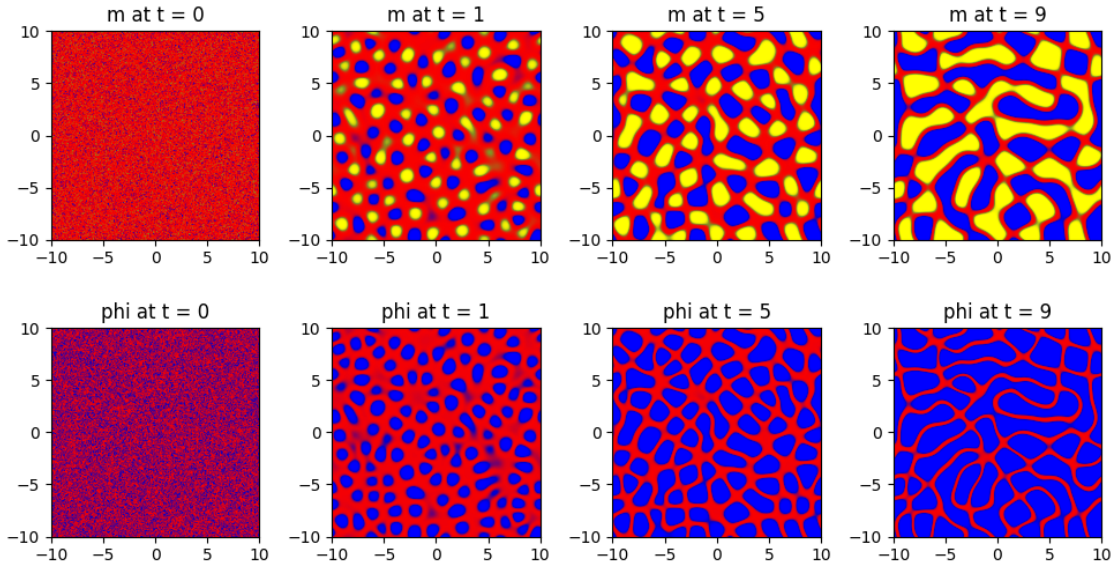


Figure 1: Simulation of equation (26) with $\alpha = 0.1$, $\beta = 10$, and initial solvent ratio of 80%. Regions where m is positive are colored blue, negative regions are colored yellow, and regions where m is near zero are colored red. Similarly, regions where ϕ is near one are colored blue whereas regions near zero are colored red.

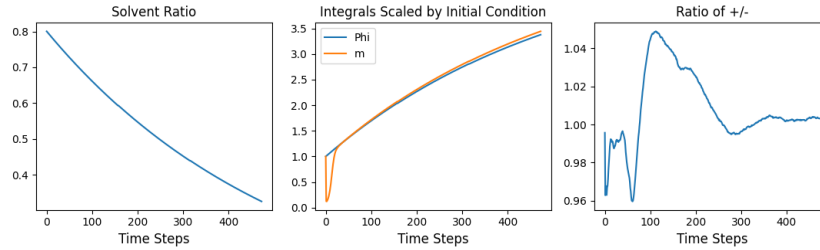


Figure 2: Solvent ratio, L^1 norms, and solute ratio of the simulation shown in Figure 1 plotted over time. The horizontal axis here represents the time step in the numerical scheme in thousands.

system (1). For instance, the study of the sharp interface via formal asymptotic expansion as done in [14, 29, 17, 1] could lead to more insight on how the morphologies grow in time. One could add further complications to this study by applying the asymptotic expansion to system (26) including the evaporation process. Another question relating to the analysis of the model is with respect to the strict separation property studied in [10, 12, 11]. Numerical simulations suggest that $\|m\| - \phi \rightarrow 0$ almost everywhere as $t \rightarrow \infty$ for initial conditions satisfying assumption (3). This property has the physical meaning that the mixture asymptotically becomes well separated and has yet to be rigorously shown.

Our main interest is to use the morphologies generated by system (1) as a type of porous domain to model and simulate charge transport under some accepted physical assumptions [28, 19]. Such simulations can allow a quantitative study of the effectiveness of the patterns of observed morphologies. With this in mind, more simulations of system (1) in three dimensions taking both perspectives of evaporation into account are crucial to best representing the physical system. Numerical schemes taking into account the gradient flow structure of the model presented in [23] similar to those studied in [16, 15] seem readily adaptable to system (1) without evaporation. As future work, we would like to study ways to include the evaporation process inside of these schemes.

Acknowledgments

The authors thank M. Eden (Karlstad, Sweden) for fruitful discussions on the mathematical analysis of the auxiliary problem and S. A. Muntean (Karlstad) for brainstorming about the modeling of the evaporation production term. RL and AM acknowledge the financial support of Carl Tryggers Stiftelse via the grant CTS 21–1656.

References

- [1] A. K. Barua, R. Chew, S. Li, J. Lowengrub, A. Münch, and B. Wagner. Sharp-interface problem of the Ohta-Kawasaki model for symmetric diblock copolymers. *Journal of Computational Physics*, 2023.
- [2] J. A. Carrillo, Y.-P. Choi, and M. Hauray. The derivation of swarming models: mean-field limit and Wasserstein distances. In A. Muntean and F. Toschi, editors, *Collective Dynamics from Bacteria to Crowds*, pages 1–46. CISM Series, 2014.
- [3] J. A. Carrillo, R. S. Gvalani, G. A. Pavliotis, and A. Schlichting. Long-time behaviour and phase transitions for the McKean–Vlasov equation on the torus. *Archive for Rational Mechanics and Analysis*, 235(1):635–690, 2020.
- [4] B. Chazelle, Q. Jiu, Q. Li, and C. Wang. Well-posedness of the limiting equation of a noisy consensus model in opinion dynamics. *Journal of Differential Equations*, 263(1):365–397, 2017.
- [5] E. N. M. Cirillo, M. Colangeli, E. Moons, A. Muntean, S. A. Muntean, and J. van Stam. A lattice model approach to the morphology formation from ternary mixtures during the evaporation of one component. *Eur. Phys. J. Spec. Top.*, 228:55–68, 2019.
- [6] C. Creton and M. Ciccotti. Fracture and adhesion of soft materials. *Reports on Progress in Physics*, 79(4):046601, 2016.
- [7] J. Cummings, J. S. Lowengrub, B. G. Sumpter, S. M. Wise, and R. Kumar. Modeling solvent evaporation during thin film formation in phase separating polymer mixtures. *Soft Matter*, 14(10):1833–1846, 2018.
- [8] M. Eden, C. Nikolopoulos, and A. Muntean. A multiscale quasilinear system for colloids deposition in porous media: Weak solvability and numerical simulation of a near-clogging scenario. *Nonlinear Analysis: Real World Applications*, 63:103408, 2022.
- [9] L. C. Evans. *Partial Differential Equations*, volume 19. American Mathematical Society, 2nd edition, 2010.
- [10] C. G. Gal, A. Giorgini, and M. Grasselli. The nonlocal Cahn–Hilliard equation with singular potential: well-posedness, regularity and strict separation property. *Journal of Differential Equations*, 263(9):5253–5297, 2017.
- [11] C. G. Gal, A. Giorgini, and M. Grasselli. The separation property for 2D Cahn–Hilliard equations: local, nonlocal and fractional energy cases. *Discrete and Continuous Dynamical Systems*, 10, 2022.
- [12] C. G. Gal and M. Grasselli. Longtime behavior of nonlocal Cahn–Hilliard equations. *Discrete & Continuous Dynamical Systems*, 34(1):145, 2014.
- [13] G. Giacomin and J. L. Lebowitz. Phase segregation dynamics in particle systems with long range interaction i. Macroscopic limits. *J. Statist. Phys.*, 87:37–61, 1997.
- [14] G. Giacomin and J. L. Lebowitz. Phase segregation dynamics in particle systems with long range interactions II: Interface motion. *SIAM Journal on Applied Mathematics*, 58(6):1707–1729, 1998.
- [15] Z. Guan, J. S. Lowengrub, C. Wang, and S. M. Wise. Second order convex splitting schemes for periodic nonlocal Cahn–Hilliard and Allen–Cahn equations. *Journal of Computational Physics*, 277:48–71, Nov 2014.

- [16] Z. Guan, C. Wang, and S. M. Wise. A convergent convex splitting scheme for the periodic nonlocal Cahn-Hilliard equation. *Numerische Mathematik*, 128(2):377–406, Oct 2014.
- [17] M. G. Hennessy, V. M. Burlakov, A. Goriely, B. Wagner, and A. Münch. Controlled topological transitions in thin-film phase separation. *SIAM Journal on Applied Mathematics*, 75(1):38–60, 2015.
- [18] H. Hoppe and N. S. Sariciftci. Organic solar cells: An overview. *Journal of Materials Research*, 19(7):1924–1945, 2004.
- [19] V. A. Khoa and A. Muntean. Corrector homogenization estimates for a non-stationary Stokes-Nernst-Planck-Poisson system in perforated domains. *Communications in Mathematical Sciences*, 17(3):705–738, 2019.
- [20] J.-M. Lasry and P.-L. Lions. Mean field games. *Japanese Journal of Mathematics*, 2(1):229–260, 2007.
- [21] W. Liu, L. Wu, and C. Zhang. Long-time behaviors of mean-field interacting particle systems related to McKean–Vlasov equations. *Communications in Mathematical Physics*, 387(1):179–214, 2021.
- [22] R. Lyons, S. A. Muntean, E. N. M. Cirillo, and A. Muntean. A continuum model for morphology formation from interacting ternary mixtures: Simulation study of the formation and growth of patterns. Technical Report arXiv:2212.12447, arXiv, December 2022.
- [23] R. Marra and M. Mourragui. Phase segregation dynamics for the Blume–Capel model with Kac interaction. *Stochastic Processes and their Applications*, 88(1):79–124, 2000.
- [24] A. Miranville. *The Cahn-Hilliard Equation: Recent Advances and Applications*. CBMS-NSF Regional Conference Series in Applied Mathematics. SIAM, 2019.
- [25] M. Müller, A. Lang, M. Klüppel, and U. Giese. Influence of phase morphology on viscoelastic properties of rubber blends. In C. Marano, F. B. Vangosa, L. Andena, and R. Frassine, editors, *Constitutive Models for Rubber XII: Proceedings of the 12th European Conference on Constitutive Models for Rubber (ECCMR 2022)*. CRC Press, 2022.
- [26] A. Muntean. *Continuum Modeling: An Approach Through Practical Examples*. SpringerBriefs in Mathematical Methods. Springer International Publishing, 2015.
- [27] S. A. Muntean, V. C. E. Kronberg, M. Colangeli, A. Muntean, J. van Stam, E. Moons, and E. N. M. Cirillo. Quantitative analysis of phase formation and growth in ternary mixtures upon evaporation of one component. *Phys. Rev. E*, 106:025306, 2022.
- [28] J. Nelson, J. J. Kwiatkowski, J. Kirkpatrick, and J. M. Frost. Modeling charge transport in organic photovoltaic materials. *Acc. Chem. Res.*, 42(11):1768–1778, 2009.
- [29] R. L. Pego. Front migration in the nonlinear Cahn-Hilliard equation. *Proceedings of the Royal Society of London. Series A, Mathematical and Physical Sciences*, 422(1863):261–278, 1989.
- [30] E. Presutti. *Scaling Limits in Statistical Mechanics and Microstructures in Continuum Mechanics*. Theoretical and Mathematical Physics. Springer, 2008.
- [31] R. Rabani, H. Sadafi, H. Machrafi, M. Abbasi, B. Haut, and P. Dauby. Influence of evaporation on the morphology of a thin film of a partially miscible binary mixture. *Colloids and Surfaces A: Physicochemical and Engineering Aspects*, 612:126001, 2021.
- [32] C. Schaefer. *Theory of nanostructuring in solvent-deposited thin polymer films*. PhD thesis, Technische Universiteit Eindhoven, 2016.
- [33] M. Setta, V. C. E. Kronberg, S. A. Muntean, E. Moons, J. van Stam, E. N. M. Cirillo, M. Colangeli, and A. Muntean. A mesoscopic lattice model for morphology formation in ternary mixtures with evaporation. *Communications in Nonlinear Science and Numerical Simulation*, 119:107083, 2023.

- [34] A. K. Tiwari, A. Pandey, J. Paul, and A. Anand. Fast accurate approximation of convolutions with weakly singular kernel and its applications, 2021. (arXiv.2107.03958).
- [35] J. M. R. Vera. A convergent iterative method for a logistic chemotactic system. *Revista Colombiana de Matemáticas*, 51(1):103–117, 2017.